Advanced methods of identification of sea-breeze and low-level jet events from near ground measurements with specific implication for energy production by offshore wind farms

Sayahnya Roy, Alexei Sentchev, Patrick Augustin, Marc Fourmentin

Advanced methods of identification of sea-breeze and low-level jet events from near ground measurements with specific implication for energy production by offshore wind farms

Sayahnya Roy[1,2] & Alexei Sentchev[1]
1. Univ. Littoral Cote d'Opale, Univ. Lille, CNRS, IRD, UMR 8187 - LOG, Laboratoire d'Océanologie et de Géosciences, F62930, Wimereux, France

2. ENSTA Paris, Institut Polytechnique de Paris, 828 Bd des Maréchaux, F-91120 Palaiseau, France

Patrick Augustin & Marc Fourmentin
Univ. Littoral Cote d'Opale, Laboratoire de Physico-Chimie de l'Atmosphère, 189A Avenue Maurice Schumann, F-59140 Dunkerque, France

ABSTRACT: Since an uniform high-speed wind is required for maximum power production, it is important to survey the meteorological phenomena which can boost up or down the power production by offshore wind turbines. The study is focused on developing and validation of advanced methods of detection of such meteorological phenomena. In situ measurements were performed at an experimental site located in Dunkirk, northern France. The wind variability was measured by Sonic anemometer during a period starting from 11th January 2018 to 18th December 2019. Automatic detection algorithms have been developed to detect sea-breeze (SB) and nocturnal low-level jet (NLLJ) events from Sonic anemometer measurements near ground. The SB detection is based on a recurrent neural network algorithm (RNN). The accuracy of event identification by this network is 95%. We found 67 and 78 SB days in 2018 and 2019 respectively. NLLJ detection algorithms developed, using wavelet transformation methods, show a better performance than other existing methods. A total of 192 and 168 NLLJ days were found in 2018 and 2019 respectively. The wind speed was found higher during the nighttime for NLLJ than for non-NLLJ days, which can increase the peak power production up to 40 times, compared to normal days. To evaluate the skill of detection algorithms based on anemometer measurements, simultaneous Sonic and lidar wind measurements have been done at site for 86-day long period. The wind speed and turbulence kinetic energy were computed from Sonic anemometer and compared to the lidar measurements. The comparison suggests that the point measurements by Sonic anemometer can be very useful for the algorithms of automatic detection of meteorological events.

1 INTRODUCTION

The lower atmospheric boundary layer in the coastal regions experiences the influence of various metrological phenomena such as sea breeze (SB), nocturnal low-level jet (NLLJ), etc. These phenomena often cause a rapid change in wind speed and direction. During SB the wind speed increases and the wind blows from the sea towards the land. This phenomenon occurs due to an adverse atmospheric pressure gradient generated by the temperature difference between land and sea (Augustin et al. 2020, Mazon et al. 2015, Roy et al. 2021b) during the daytime.

During clear weather, after sunset, a strong wind acceleration can be observed around 50-1000 m above ground level (a.g.l.), known as NLLJ (Roy et al., 2021a, Smedman et al. 1996). Moreover, the properties of NLLJ are influenced by horizontal temperature gradients between land and sea, elevated turbulence level, etc (Källstrand 1998; Kallistratova et al. 2013). Recently the offshore wind energy became largely exploitable in many countries. Since the SB is a frequent event in the coastal and offshore wind climate, it can

significantly affect the resource assessment during the initial pre-construction phase of offshore wind farms. To explore the impact of SB on power production by wind turbines, some studies were done in the North Sea (Steele et al. 2013, 2015) and an enhancement of energy due to SB was observed. During the SB event, the estimated energy production can be increased by 15% (Kumar et al. 2021), but an adverse effect of turbulence on wind turbine blades was found by Mazon et al. (2015). Garvine et al. (2008) stated that SB events are very effective to fulfil the power requirement from offshore wind farms.

To achieve the nighttime power requirement from offshore wind farms, NLLJ event can be effective in coastal ocean regions. In the Dutch part of the North Sea, an occurrence of a small boundary layer deepening due to the NLLJ was observed, which can be useful for enhanced power production (Baas et al. 2005, Duncan 2018). Greene et al. (2009) observed that average power production is larger during NLLJ day compared to that of for non-NLLJ day. Further,

Figure 1. Measurement locations.

Wilczak et al. (2015) reported that the capacity factor of a wind turbine (ratio between average power output and maximum power capability) increases by 60% during the NLLJ events.

Since the wind turbine output power is proportional to the cube of hub-height wind speed, errors in wind speed forecasting can significantly affect the wind power forecasts. Such errors are not only costly in terms of ensuring adequate energy supplies to the customer, but over-or underestimations of power production can also have a considerable related financial cost. Therefore, there is a strong motivation to fully understand the offshore wind climate. To do this we need some advanced algorithms to detect the SB and NLLJ events efficiently and quickly.

This study is focused on the development of some cutting-edge classification algorithms for SB and NLLJ using time series of wind speed, wind direction, turbulence kinetic energy, measured by a Sonic anemometer in the coastal region of northern France. Also, we have checked the performance of these algorithms by comparing them with lidar measurements. In the literature, several methods of SB detection were proposed. The are based on time series classification, such as feature-based (Nanopoulos et al. 2001), ensemble based (Bagnall et al. 2015, Koley and Dey 2012), and deep learning approach (Wang et al. 2017, Cui et al. 2016). However, no studies were focused on the development of SB day classification algorithms using machine learning. The objective of this study is to develop a new machine learning algorithm using a recurrent neural network (RNN) to detect SB days. Also, another algorithm is used for detection of NLLJ using discrete wavelet transform. The measurements used for validation of our algorithms are presented in section 2. Methodology of analysis and classification is given in section 3. The results are summarized in section 4, followed by the conclusion in section 5.

2 MEASUREMENTS

Figs. 1 show the measurement locations. Measurements have been done in Dunkirk for 2 years period (2018-2019) using the Sonic anemometer. The measurement device provides 15 minutes averaged data of turbulence parameters. Additionally, the lidar and 20 Hz Sonic anemometer measurements have been done simultaneously for 86 days period (from July to October 2021) to assess the impact of NLLJ and SB on turbulence kinetic energy of the flow field near the ground.

3 METHODOLOGY

3.1 *Calculation of turbulence parameters*

Let us assume u_R, v_R and w_R are the zonal, meridional and vertical components of wind velocity measured using the Sonic anemometer.. To avoid the effect of meteorological coordinate system on the turbulence parameters estimation, we have adopted a new coordinate system where the mean flow is aligned with the *x*-axis (Roy et al. 2021b, Golzio et al. 2019). In the new coordinate system, the instantaneous streamwise, transverse, and vertical wind velocity components (*u*, *v*, and *w*) were decomposed into a mean part and fluctuating part as:

$$u = \overline{u} + u', v = \overline{v} + v', w = \overline{w} + w' \quad (1)$$

where $\overline{u}, \overline{v},$ and $\overline{w}$ are the mean velocity components (15 min averaged), and $u', v',$ and w' are the corresponding velocity fluctuations.

The turbulence kinetic energy (TKE) is defined as:

$$TKE = \frac{1}{2}\left(\overline{u'^2} + \overline{v'^2} + \overline{w'^2}\right) \quad (2)$$

3.2 *Identification methods*

To detect the SB, and NLLJ, we have developed four automatic detection algorithms referred to hereafter as M1, NM2, WM3, and WM4 (defined in Table 1). These algorithms were designed for analysis of static point measurements.

Table 1. Methods used for identification of meteorological phenomena by four algorithms applied for analysis of Sonic anemometer data.

Methods	developed algorithms
M1	sign change of sea breeze component
NM2	recurrent neural network (RNN) for sea-breeze component (SBC)
WM3	haar wavelet threshold technique for NLLJ
WM4	symlets wavelet slope technique for NLLJ

In the M1 algorithm, four filters were used to identify the SB days (step 1 to 4 in Fig. 2). Step-1 separates the extreme event. In Step-2, during a period from 08:00 to 11:00 UTC, a shift in wind direction from offshore to onshore was recognized from an alteration of the sign of the normalized SB component ($SBC=(U\times sin(0-W_D))/U$), where W_D is the wind direction and U is the horizontal wind speed), from negative to positive value of SBC signify the SB day. In the last step, a positive slope of the temperature gradient confirms the authenticity of the SB day.

In NM2 framework, the Long short-term memory (LSTM) neural networks are a typical form of recurrent neural network (RNN). Hidden units in LSTM are capable of recalling the long-term memory in sequential data (e.g., time series data), lead to enhance the efficiency to classify the SB and non-SB days. Fig. 3 shows the LSTM framework of method NM2. Since, SB days are frequent during the summer, we have used six months of data (from April to September) in the input layer. The SBC in each day treated as features, which consist of 15 minutes averaged wind direction for a period of 24 hours. 182 sequential feature vectors are used to train the network. The cell state in one LSTM block is updated by four interacting layers demonstrated as: forgetting gate, input gate, cell state updating and output gate. Equations involves in these gates are detailed in (Roy et al., 2021, Goodfellow et al., 2016). Note that a number of

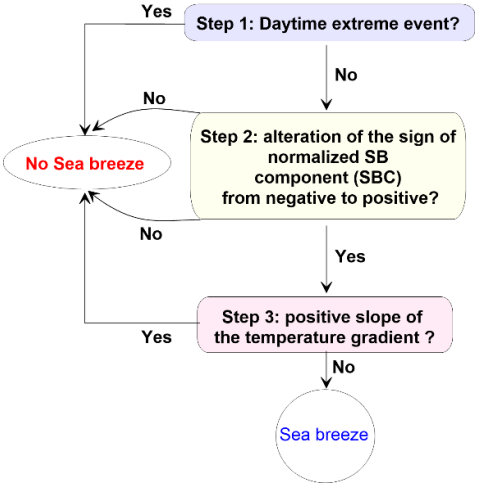

Figure 2. Conceptual scheme for the sea-breeze identification method M1.

trials with hidden units were made to optimize the hyperparameter. We found that 96 hidden units allows the optimal prediction of SB days. The Output from LSTM pass through a fully connected layer (2 classes). The output from fully connected layer is followed by output layer and consists of softmax activation function leading to classification as binary (i.e. 1 for SB or 0 for non SB).

We have used cross-entropy loss function to train classifiers. To optimize the backpropagation, the Adaptive Momentum Estimator (ADAM) is used. To train the network, we have used 182 sequences from the year 2018. To test the network output, same number of sequences from the year 2019 is used.

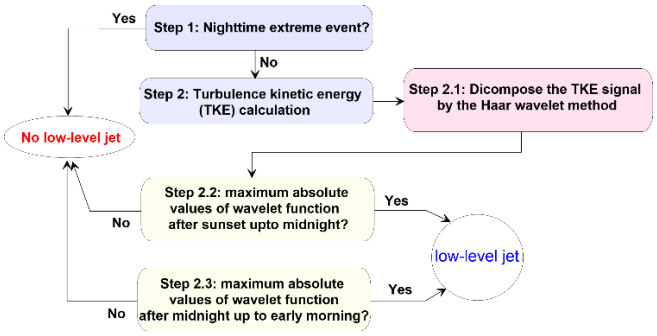

Figure 4. Conceptual scheme for the low-level jet identification method WM3 using haar wavelet function.

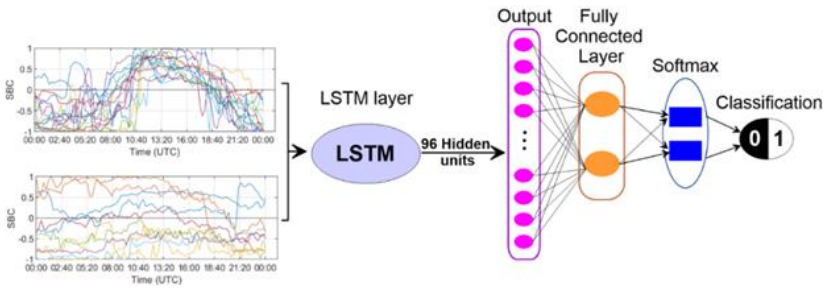

Figure 3. Recurrent neural network for the sea-breeze identification method NM2.

Fig. 4 shows the conceptual scheme for WM3, where we have used 5 filters (steps 1 to 2.3) to identify the NLLJ event. Since the LLJ is a nighttime event, Step-1 eliminates the extreme events. The turbulence kinetic energy (TKE) is calculated in Step-2. The decomposition of TKE is done by the Haar wavelet function (Baars et al., 2008, Augustin et al., 2020) in Step-2.1. In steps-2.2 and 2.3, maximum absolute values of wavelet function after sunset up to early morning signifies the occurrence of NLLJ.

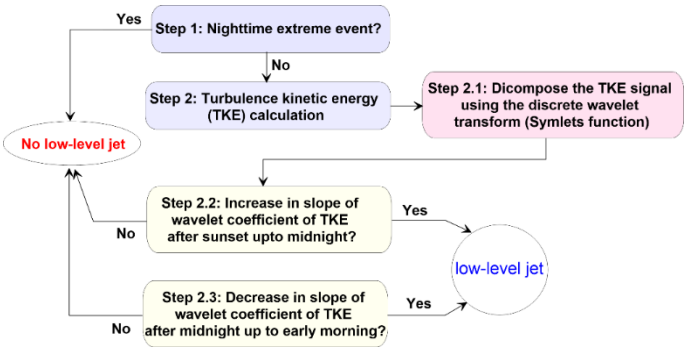

Figure 5. Conceptual scheme for the low-level jet identification method using symlets wavelet function and slope of wavelet coefficients (WM4).

The conceptual scheme for WM4 is shown in Fig. 5. Steps-1 and 2 used in this algorithm are exactly the same as WM3. But the decomposition of the TKE signal is done by discrete wavelet transform. Symlets mother wavelet function (Al-kadi et al., 2012) is used to decompose the TKE signal into 4 levels of time resolutions (15 minutes to 1 hour). We have tried to identify the NLLJ with all resolutions of decomposed TKE signals and found that a 1-hour resolution (level 4) of the TKE signal provides the optimal classification. The slope of this decomposed TKE has been computed after sunset up to early morning. In steps- 2.2 and 2.3, if the slope is positive from morning to midnight and negative from midnight to early morning considered as an NLLJ event otherwise non NLLJ event.

4 RESULTS AND DISCUSSION

4.1 *Seabreeze classification results*

The daytime heating creates thermal instability between land and sea, resulting in a concentrated wind flow from the sea toward land. We found 67 and 78 SB days in 2018 and 2019 respectively during the summertime (Fig.6 a and b) using M1 algorithm. Furthermore, we have developed a NM2 algorithm using LSTM block capable of detecting SB days. To train the network we have used the categorical SBC data from 2018. Trained network (NM2) is used to classify the SB days in 2019.

The average actual and predicted SBC for all SB days are shown in Fig. 7 a and Fig. 7 b respectively. To check the classification performance of the NM2 algorithm, three statistical metrics were used: sensitivity, specificity, and classification accuracy (Fig. 7 c).

The sensitivity is defined as the ratio between classified true positive (i.e., both observation and prediction samples are positive) and the total number of

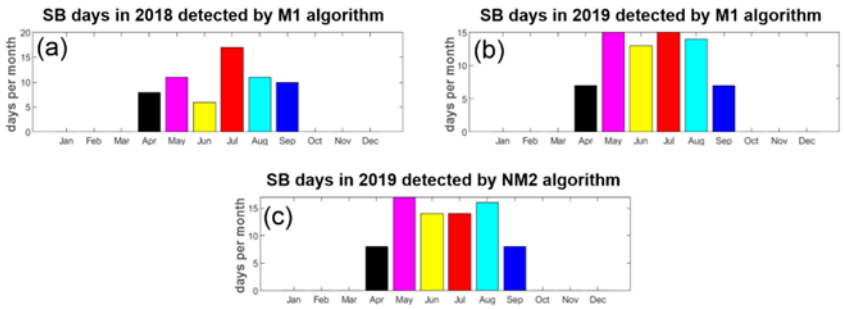

Figure 6. Identification of SB days using M1 algorithm from wind measurements in 2018 (a), 2019 (b). SB days identified by NM2 algorithm.

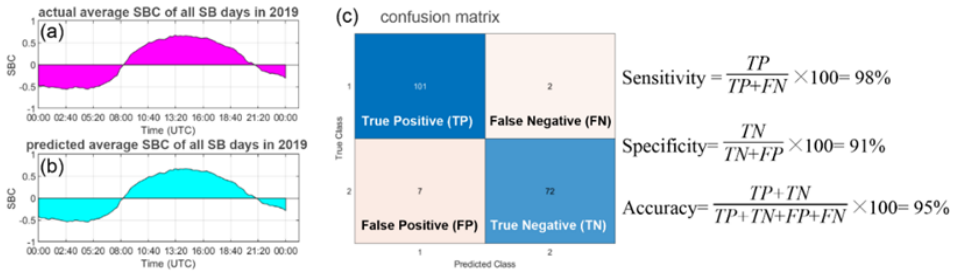

Figure 7. performance test of NM2 algorithm for SB days identification in 2019, actual average SBC of all SB days (a), predicted average SBC of all SB days (b), confusion matrix and accuracy (c).

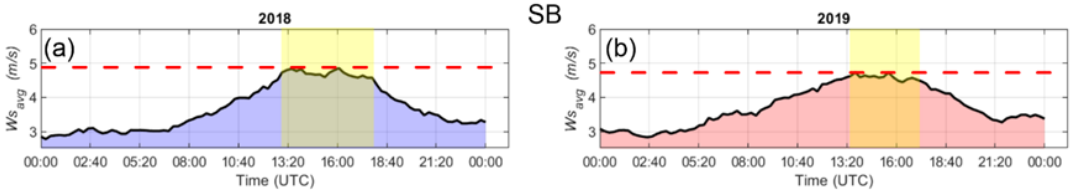

Figure 8. Average of wind speed (Ws_{avg}) for all SB days during 2018 (a), 2019 (b).

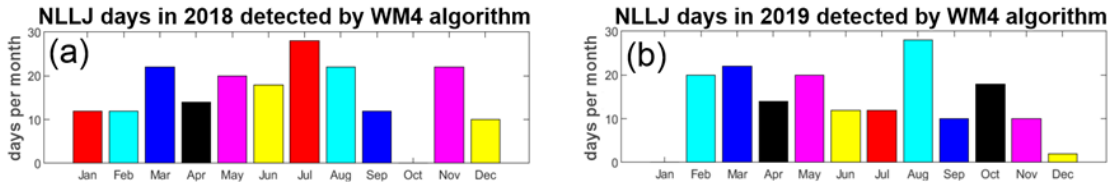

Figure 9. Identification of NLLJ days using WM4 algorithm from wind measurements in 2018 (a), 2019 (b)

samples in true class 1, where false negative signifies the observed samples are positive but prediction samples are negative. Specificity can be stated as the proportion between true negative (i.e., both observation and prediction samples are negative) and the total number of samples in true class 2, where false positive means the observed samples are negative but prediction samples are positive. The accuracy is calculated as the ratio of true positive and negative samples with all classes. The proposed NM2 algorithm is good enough with sensitivity = 98%, specificity = 91%, and classification accuracy = 95%. The performance of the NM2 algorithm can be enhanced with a greater number of observations.

Fig. 8 shows the average wind speed of all SB days as a function of time (UTC). For both years, the range of average wind speed L_{ws}=2.9 m/s to H_{ws}=4.9 m/s is quite similar (Figs. 8a and b), here L_{ws} and H_{ws} is low and high wind speed respectively. The maximum wind speed during the SB days occurs roughly from 13:00 UTC to 17:30 UTC in both years. We have observed that the maximum average wind speed during SB events is around 5 m/s (a.g.l. 10 m).

4.2 *Nocturnal low-level jet classification results*

A concentrated wind flow after sunset is known as the NLLJ. Since the NLLJ is a nighttime phenomenon, it can increase offshore wind power production during the nighttime. Therefore, it is important to detect the NLLJ phenomenon in coastal regions where offshore wind turbines are installed. We have developped two automatic NLLJ detection algorithms WM3 and WM4. Since the performance of both algorithms is quite similar for the NLLJ classification, we present the results obtained only by WM4 in Fig. 9.

From Figs. 9 a and b it is quite difficult to make any concrete discussion about the season of maximum NLLJ occurrence. Except for October 2018 and January 2019, we found a significant occurrence of NLLJ every month. A total of 192 and 168 NLLJ were found in 2018 and 2019 respectively.

4.3 *Comparative study between the Sonic and lidar measurements*

All the identification algorithms are developed using Sonic anemometer measurements (15 minutes averaged) at 10 m a.g.l. Since the range of height of offshore wind turbines is generally from 80m to150m, it is necessary to check if there is some significant signature of meteorological events occurring at the altitude in the near-ground measurements. To check it, simultaneous measurements have been performed using a 20 HZ Sonic anemometer (at 10 m a.g.l.) and a lidar measurements (spatial range from 40m to 300 m a.g.l.) in Dunkirk for 86 days from 23/07/2021 to 16/10/2021.

During this measurement period, we found the occurrence of NLLJ approximately every night. We found 2 SB days from 23/07/2021 to 31/07/2021 8 days in August, and 10 days in September 2021. Note that we have selected three representative days to compare the Sonic and lidar measurements, 07/09/2021 for NLLJ,21/09/2021 for SB day, and 07/10/2021 for a normal day. Note that, though we found the NLLJ at 18:00 and 22:00 to 24:00 UTC on 07/10/2021 we can ignore this period as the intensity of the NLLJ was very small. To compare all the events, we have selected the period starting from 00:00 to 18:00 UTC as a normal day.

Figs. 10a, b and c show the horizontal wind speed variation as a function of time and height. We found NLLJ during 18:00 to 24:00 UTC (Fig. 10a), SB during 11:00 to 16:00 UTC (Fig. 10b).

Estimation of the power production is performed using the velocity data. We have calculated the power as $Power = \pi/2\,(r^2U^3\rho\varphi)$, where r is the rotor ra-

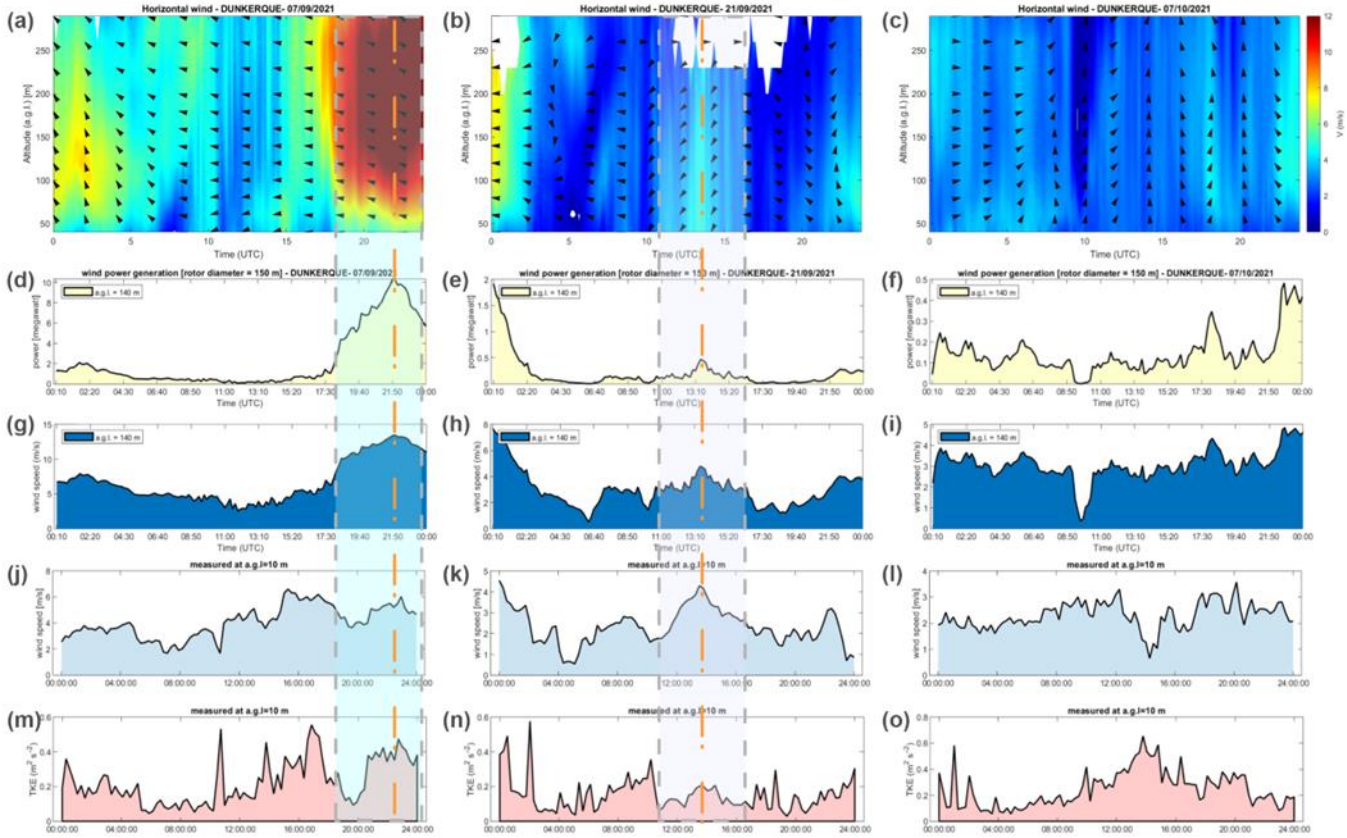

Figure 10. First row: wind speed and direction from lidar measurement for three atmospheric conditions: NLLJ, SB, normal day condition (a, b, c); Second row: expected power at 140m a.g.l. for three conditions (d, e, f); Third row: wind speed at 140m a.g.l. for three conditions (g, h, i); Fourth row: wind speed from Sonic measurement for same conditions at a.g.l. = 10 m (j, k, l); TKE at a.g.l. = 10 m for same conditions (m, n, o). Shaded portion bounded by gray dashed line shows the periods of LLJ and SB events. Dashed dot lines correspond to the peak power production during LLJ and SB events.

dius, U is the wind speed at a.g.l.= 140 m, ρ is the air density, φ is the efficiency factor, we have used φ=40% for all calculations. Fig. 10d shows that the maximum power (10 megawatts) can be achieved at 22:00 UTC during the NLLJ event. We found an increase in power at 13:30 UTC during the SB event (Fig. 10e). However during the NLLJ event, the estimated peak power generation is approximately 20 times higher than that during the SB event (Fig. 10e). It is observed from Fig. 10d that estimated power generation starts to increase from the initiation of LLJ (18:00 UTC), then it achieved a peak at 22:00 UTC, and it starts to decrease from 22:00 to 24:00 UTC. For the SB period (11:00 to 16:00 UTC) the estimated power variation shows a similar evolution.

Comparison between the wind speed U at 140 m and 10 m a.g.l. suggests that during the NLLJ U at 140m is 2 times larger (Figs. 10g and j). The variability of U suggests the existence of a jet shear layer at 10 m and jet core at 140 m a.g.l. However, U obtained at two altitudes, 10 m and 140 m a.g.l., is similar during the SB event (Figs. 10h and k), which signifies that the SB can develop an internal boundary layer near the ground. It is hard to find a correlation between U at two altitudes during a normal day.

The TKE shows a time variability similar to that of wind speed U during the NLLJ and SB events (Figs. 10 m, n). By comparing all parameters in Fig. 10 it is found that wind variability at a.g.l. 140 m and 10 m is similar, thus Sonic anemometer measurements can be useful to identify LLJ and SB events.

5 CONCLUSIONS

In this study, we assessed the wind measurements aiming at identifying various meteorological events in Dunkirk prior to offshore wind farm installation there. Measurements have been done using a Sonic anemometer and wind lidar in the coastal region of Dunkirk. We found that the peak wind speed is 4 times and 1.5 times higher during NLLJ and SB events respectively than that for normal days. The wind speed during SB can boost the average energy production by approximately 15% than non-sea breeze days. The SB can increase 2 times the energy production at sites close to the shore compared to sites located far from the shore. During the nighttime the wind speed is higher for NLLJ than non-NLLJ days, which can increase the peak power production up to 40 times compared to normal days. Therefore, the quantification of the occurrence of NLLJ and SB

days in a year is important for wind energy resource assessment. We have developed four algorithms to identify NLLJ and SB days based on: sign change of the sea breeze component (M1), recurrent neural network (RNN) also for SBC (NM2), haar wavelet threshold technique for NLLJ (WM3), and symlets wavelet slope technique for NLLJ (WM4).

These algorithms identified the SB and NLLJ days successfully. Some significant results obtained from the analysis are the following:

1. The proposed NM2 algorithm is good enough for SB identification with sensitivity = 98%, specificity = 91%, and classification accuracy = 95%.

2. For NLLJ detection, both WM3 and WM4 algorithms give very good and nearly identical results (99% of similarity).

3. During the NLLJ and SB events the estimated peak power generation is approximately 40 and 2 times higher than that of a normal day respectively.

4. Comparison between wind speed at 140 m and 10 m a.g.l. suggests that during NLLJ, the wind speed at 140m is 2 times larger than that at 10 m a.g.l. However, the wind speed obtained at both levels is similar during the SB event due to the formation of internal boundary layer.

REFERENCE

1. Al-kadi, M.I., Reaz, M.B.I. and Ali, M.M., 2012, December. Compatibility of mother wavelet functions with the electroencephalographic signal. In 2012 IEEE-EMBS Conference on Biomedical Engineering and Sciences (pp. 113-117). IEEE.
2. Augustin, P., Billet, S., Crumeyrolle, S., Deboudt, K., Dieudonné, E., Flament, P., Fourmentin, M., Guilbaud, S., Hanoune, B., Landkocz, Y. and Méausoone, C., 2020. Impact of sea breeze dynamics on atmospheric pollutants and their toxicity in industrial and urban coastal environments. Remote Sensing, 12(4), p.648.
3. Augustin, P., Delbarre, H., Lohou, F., Campistron, B., Puygrenier, V., Cachier, H. and Lombardo, T., 2006, November. Investigation of local meteorological events and their relationship with ozone and aerosols during an ESCOMPTE photochemical episode. In Annales Geophysicae (Vol. 24, No. 11, pp. 2809-2822). Copernicus GmbH.
4. Baars, H., Ansmann, A., Engelmann, R. and Althausen, D., 2008. Continuous monitoring of the boundary-layer top with lidar. Atmospheric chemistry and Physics, 8(23), pp.7281-7296.
5. Baas, P., Bosveld, F.C., Klein Baltink, H. and Holtslag, A.A.M., 2009. A climatology of nocturnal low-level jets at Cabauw. Journal of Applied Meteorology and Climatology, 48(8), pp.1627-1642.
6. Bagnall, A., Lines, J., Hills, J. and Bostrom, A., 2015. Time-series classification with COTE: the collective of transformation-based ensembles. IEEE Transactions on Knowledge and Data Engineering, 27(9), pp.2522-2535.
7. Crumeyrolle, S., Augustin, P., Rivellini, L.H., Choël, M., Riffault, V., Deboudt, K., Fourmentin, M., Dieudonné, E., Delbarre, H., Derimian, Y. and Chiapello, I., 2019. Aerosol variability induced by atmospheric dynamics in a coastal area of Senegal, North-Western Africa. Atmospheric Environment, 203, pp.228-241.
8. Cui, Z., Chen, W. and Chen, Y., 2016. Multi-scale convolutional neural networks for time series classification. arXiv preprint arXiv:1603.06995.
9. Duncan, J.B., 2018. Observational analyses of the North Sea low-level jet. Petten: TNO.
10. Goodfellow, I., Bengio, Y. and Courville, A., 2016. Deep learning. MIT press.
11. Garvine, R.W. and Kempton, W., 2008. ssessing the wind field over the continental shelf as a resource for electric power. Journal of Marine Research, 66(6), pp.751-773.
12. Golzio, A., Bollati, I.M. and Ferrarese, S., 2019. An assessment of coordinate rotation methods in Sonic anemometer measurements of turbulent fluxes over complex mountainous terrain. Atmosphere, 10(6), p.324.
13. Greene, S., McNabb, K., Zwilling, R., Morrissey, M. and Stadler, S., 2009. Analysis of vertical wind shear in the Southern Great Plains and potential impacts on estimation of wind energy production. International journal of global energy issues, 32(3), pp.191-211.
14. Källstrand, B., 1998. Low level jets in a marine boundary layer during spring. Contributions to atmospheric physics, 71.
15. Kallistratova, M.A., Kouznetsov, R.D., Kramar, V.F. and Kuznetsov, D.D., 2013. Profiles of wind speed variances within nocturnal low-level jets observed with a sodar. Journal of Atmospheric and Oceanic Technology, 30(9), pp.1970-1977.
16. Koley, B. and Dey, D., 2012. An ensemble system for automatic sleep stage classification using single channel EEG signal. Computers in biology and medicine, 42(12), pp.1186-1195.
17. Kumar, R., Stallard, T. and Stansby, P.K., 2021. Large-scale offshore wind energy installation in northwest India: Assessment of wind resource using Weather Research and Forecasting and levelized cost of energy. Wind Energy, 24(2), pp.174-192.
18. Mazon, J., Rojas, J.I., Jou, J., Valle, A., Olmeda, D. and Sanchez, C., 2015. An assessment of the sea breeze energy potential using small wind turbines in peri-urban coastal areas. Journal of Wind Engineering and Industrial Aerodynamics, 139, pp.1-7.
19. Nanopoulos, A., Alcock, R. and Manolopoulos, Y., 2001. Feature-based classification of time-series data. International Journal of Computer Research, 10(3), pp.49-61.

20. Roy, S., Sentchev, A., Schmitt, F.G., Augustin, P. and Fourmentin, M., 2021a. Impact of the Nocturnal Low-Level Jet and Orographic Waves on Turbulent Motions and Energy Fluxes in the Lower Atmospheric Boundary Layer. Boundary-Layer Meteorology, pp.1-16.
21. Roy, S., Sentchev, A., Fourmentin, M. and Augustin, P., 2021b. Turbulence of Landward and Seaward Wind during Sea-Breeze Days within the Lower Atmospheric Boundary Layer. Atmosphere, 12(12), p.1563.
22. Roy, S., 2021c. Multi-step wind variability prediction based on deep learning neural network. In EGU General Assembly Conference Abstracts (pp. EGU21-1487).
23. Smedman, A.S., Högström, U. and Bergström, H., 1996. Low level jets–a decisive factor for off-shore wind energy siting in the Baltic Sea. Wind Engineering, pp.137-147.
24. Steele, C.J., Dorling, S.R., Glasow, R.V. and Bacon, J., 2013. Idealized WRF model sensitivity simulations of sea breeze types and their effects on offshore windfields. Atmospheric Chemistry and Physics, 13(1), pp.443-461.
25. Steele, C.J., Dorling, S.R., von Glasow, R. and Bacon, J., 2015. Modelling sea-breeze climatologies and interactions on coasts in the southern North Sea: implications for offshore wind energy. Quarterly Journal of the Royal Meteorological Society, 141(690), pp.1821-1835.
26. Wang, Z., Yan, W. and Oates, T., 2017, May. Time series classification from scratch with deep neural networks: A strong baseline. In 2017 International joint conference on neural networks (IJCNN) (pp. 1578-1585). IEEE.
27. Wilczak, J., Finley, C., Freedman, J., Cline, J., Bianco, L., Olson, J., Djalalova, I., Sheridan, L., Ahlstrom, M., Manobianco, J. and Zack, J., 2015. The Wind Forecast Improvement Project (WFIP): A public–private partnership addressing wind energy forecast needs. Bulletin of the American Meteorological Society, 96(10), pp.1699-1718.